Mechanical and textural properties of pelvic trabecular bone

J. Biomechanics Vol. 26, No. 4/5, pp. 523–535, 1993.
Printed in Great Britain

0021–9290/93 $6.00+.00

MECHANICAL AND TEXTURAL PROPERTIES OF PELVIC TRABECULAR BONE*

M. DALSTRA,† R. HUISKES,†‡ A. ODGAARD§ and L. VAN ERNING‖

†Biomechanics Section, Institute of Orthopaedics, University of Nijmegen, Nijmegen, The Netherlands; §Biomechanics Laboratory, Orthopaedic Hospital, University of Aarhus, Aarhus, Denmark; and ‖Institute of Diagnostic Radiology, St Radboud University Hospital Nijmegen, Nijmegen, The Netherlands

Abstract—So far, virtually nothing is known about the mechanical properties of pelvic trabecular bone. In this study, several techniques have been used to establish some insight in these properties. Dual-energy quantitative computer tomography (DEQCT) was used to look at the distribution of bone densities throughout the pelvic bone and nondestructive mechanical testing was used to obtain Young's moduli and Poisson's ratios in three orthogonal directions for cubic specimens of pelvic trabecular bone. The same specimens were then used for stereological measurements to obtain volume fractions and the spatial orientations of the mean intercept lengths. The combined data on the mechanical tests and the stereological measurements made it possible to calculate Young's moduli and Poisson's ratios for the specimens' principal material axes.

DEQCT showed that bone densities within a pelvic bone are significantly higher in the superior part of the acetabulum, extending to the sacroiliac joint area and, secondly, in the area of the pubic symphysis. Volume fractions found for the specimens did not exceed 20%. This may be considered rather low when compared to values reported in the literature for trabecular bone of femoral or tibial origin, but the values do lie in the same range as vertebral trabecular bone. With the volume fraction as its primary predictor, values of Young's moduli were also low. For most specimens these values were not higher than 100 MPa, with an occasional peak of 250 MPa. Looking at the ratio of the highest and lowest Young's modulus or at the components of the fabric tensor, it can be concluded that pelvic trabecular bone is not highly anisotropic. On an average, Poisson's ratio was found to be closer to 0.2 rather than 0.3, which is in accordance with other studies on Poisson's ratio of trabecular bone.

INTRODUCTION

Being part of the hip joint, the pelvic bone, like its femoral counterpart, frequently appears in finite element studies. However, apart from the obvious anatomical differences, there is another striking difference between the femur and the pelvic bone. Mechanical properties of femoral bone are well documented, but it is somewhat surprising that on the mechanical properties of pelvic bone virtually no data exist. The pelvic bone mainly consists of trabecular bone covered by a thin layer of cortical bone. Young's moduli used in various finite element studies of pelvic trabecular bone vary from 40 to 3000 MPa. For the most part, these values were based on experimental data of tibial and femoral origin. Only Vasu *et al.* (1982) and Rapperport *et al.* (1985) used density observations from roentgenograms to estimate Young's moduli. In all the studies, bone was assumed to be isotropic. Vasu *et al.* (1982), Pedersen *et al.* (1982) and Rapperport *et al.* (1985) made a differentiation in the values of Young's modulus, based on density distributions, whereby near the acetabulum the density was found to be the highest and decreasing in value further away from the acetabulum. In most finite element studies, the Poisson's ratio for pelvic trabecular bone was taken as 0.2. Only Goel *et al.* (1978) and Pedersen *et al.* (1982) assumed a value of 0.3. Again, however, measurements for this value were never made.

Because of its sandwich construction, the overall mechanical behavior of the pelvic bone is to some extent insensitive to variations of the mechanical properties of its trabecular bone (Dalstra and Huiskes, 1990). However, if stresses and strains in the trabecular bone itself are the subject of study, accurate values of its material properties will be a prerequisite. Therefore, the purpose of the present study was to obtain a better insight into the material properties of pelvic trabecular bone. To achieve this, three different techniques were used. With dual-energy quantitative computer tomography, trabecular bone densities were quantified throughout the pelvic bone. This was necessary as the dimensions of the specimens used for mechanical testing limit harvesting to only those areas which have sufficient bone stock. Mechanical testing of pelvic trabecular bone specimens was performed in three orthogonal directions; thus, not only providing values of Young's moduli and Poisson's ratios, but also information about the degree of anisotropy. Finally, using a three-dimensional reconstruction technique, stereological measurements were performed on the same specimens used for mechanical testing, in order to identify the material's principal

Received in final form 11 *September* 1992.

*Partly presented at the 38th Annual Meeting of the Orthopaedic Research Society, 17–20 February 1992, Washington DC, U.S.A.

‡Author to whom correspondence should be addressed at: Biomechanics Section, Institute of Orthopaedics, University of Nijmegen, P.O. Box 9101, 6500 HB Nijmegen, The Netherlands.

directions and, together with the data from the mechanical tests, to calculate the elastic constants in those directions.

METHODS AND MATERIALS

Material

For dual-energy quantitative computer tomography (DEQCT), six right pelvic bones were available: one of a 78-year-old male and five of females, ranging from 77 to 87 years. Being embalmed, these bones were not used for mechanical testing. For this purpose, two fresh right pelvic bones were used; one of a 82-year-old female and one of a 72-year-old male. None of the donors was known to have a history of bone or joint disease. From each bone, as many cubic specimens as possible were taken. Due to its smaller size, the bone of the female donor yielded no more than 18 specimens. From the other bone, 39 specimens could be obtained. Due to insufficient bone stock in both bones, no specimens could be taken from the superior iliac crest, nor from the connection between ischial and pubic bone. All cubes were cut according to a Cartesian coordinate system defined by a plane over the rim of the acetabulum (the *xy*-plane, the *x*-axis bisecting the angle between the ischial and pubic bones) and the *z*-axis as the normal to this plane, pointing into the acetabulum. The cubes were machined on a cutting–grinding system (EXAKT cutting–grinding system). Different colors of dye were used to mark the orientation of the faces of the bone cubes. These cubes had sides of about 6.5 mm; the exact dimensions of each individual specimen were measured with a caliper. After cutting, the specimens were stored in a wet state at $-18°C$ until testing.

Quantitative computer tomography

The bones were scanned with a CT-scanner (Siemens, SOMATOM DR3) using dual energy mode, i.e. at 85 and 125 kVp. Using the same definition of the coordinate axes as mentioned above, scans were taken parallel to the *yz*-plane. Slice thickness was 8 mm and the distance between two consecutive scans was 10 mm. This resulted in 21 or 22 scans per bone, depending upon the size. Together with the bones, a calibration phantom (Kalender and Suess, 1987) was scanned in order to be able to relate the X-ray absorption values with their Ca-equivalents. Post-processing the CT-data, calcium images were reconstructed, which were used for further evaluation. Via a network, the digital images were transferred to a PC. Using a PC-based image-analysis system (TIM, Difa Measuring Systems, Breda, The Netherlands), the areas of trabecular bone in each scan were marked and the average Ca-equivalents for those areas were calculated, thus providing a global mapping of trabecular bone densities throughout a pelvic bone. Furthermore, Ca-equivalents were measured locally at the same places where the cubic specimens had been harvested, which should give information about the relation between apparent density and Ca-equivalent density.

Mechanical testing

Unconstrained compressive mechanical testing was performed on a 4302 model Instron materials testing machine (INSTRON Ltd., High Wycombe, Bucks., U.K.). As several tests had to be performed on one specimen in order to obtain the material properties in the three directions of the cube, a nondestructive test procedure was used (Linde *et al.*, 1988). All tests were performed at a strain rate of 0.1% s^{-1} up to a maximal strain of 0.8%. Before the actual test cycle, the bone samples were conditioned to viscoelastic steady state by uniaxial cyclic compression between preloads of 2 N (defined as 0% strain) and 0.8% strain. Usually, 5–10 cycles were necessary to reach steady state. During the actual test, the longitudinal deformation was recorded by an extensometer, fixed to the anvils as close to the specimen as possible, and the deformation in one of the transverse directions was recorded by a pair of LVDTs, placed opposite to one another. In measuring the transverse deformation, the surfaces were covered by a plastic foil. After one test cycle, the specimen was rotated 90° around its longitudinal axis and tested once more to measure the other transverse deformation. This procedure was repeated for the longitudinal axis set to each of the three directions, resulting in a total of six test cycles for each specimen. The order in which each axis was chosen to be the longitudinal axis (*xyz*) was the same for each specimen, although this does not seem to have a major effect on the stiffness values (Linde *et al.*, 1990b).

Load and deformation data were recorded during testing and sent to a PC, where they were converted into stress and strain values. A 5th-degree polynomial fitting routine was performed on the stress data as a function of the longitudinal strain and on the transverse strain data as a function of the stress. Then the stress and the accompanying transverse strain were calculated at a longitudinal strain of 0.7%. The elastic modulus was defined as the tangent of the stress curve at a longitudinal strain of 0.7% and Poisson's ratio as the ratio between the transverse strain and the longitudinal strain. For the second test in the same longitudinal direction, the same routine was followed and then the two elastic moduli were averaged. This was performed for all there directions of the cube, finally resulting in three elastic moduli and six Poisson's ratios for a single specimen.

After testing, the marrow was removed from the specimens by air jet and subsequently specimens were submerged in an alcohol/acetone solution for 2 days. After a final air jet cleansing and a one day evaporation time, the specimens were weighed. The apparent density of a specimen was then calculated from the weight of the specimen and its volume.

Stereological measurements

Data from the mechanical tests, by itself, are not sufficient to calculate all elastic constants, as beforehand, unlike for the trabecular bone in the proximal tibia, no information is available on the direction of the material's principal axes. However, assuming that the axes of the mean intercept length (MIL) ellipsoid coincide with the principal axes of the material (Harrigan and Mann, 1984), it becomes possible to reconstruct the elasticity (or compliance) matrix in its principal directions. The only flaw in this assumption is that if the principal axes should happen to coincide with the directions in which mechanical testing was performed, the calculated values for the shear moduli will not be very good.

To be able to perform true three-dimensional MIL measurements, a three-dimensional series reconstruction technique was used (Odgaard *et al.*, 1990). Due to technical reasons, only the specimens of the male pelvic bone were used for the MIL measurements. Of the original 39, six cubes failed during the embedding process, leaving 33 cubes for stereological analysis. Figure 1 shows the locations on the pelvic bone from where these specimens were taken. The specimens were imbedded in a black epoxy resin under vacuum. Using a standard hard tissue microtome, the specimens were sectioned, whereby an image of the section was digitized by a CCD camera mounted on the microtome. Depending upon the exact size of the specimen, around 300 images of the individual sections were thus obtained and their binary information was stored after segmentation. From these files, a three-dimensional array consisting of voxels representing either bone or 'air', could then be reconstructed.

The volume fraction of bone was calculated simply by dividing the number of voxels representing bone by the total number of voxels. The MIL was measured by defining 222 uniformly random sets of equally spaced parallel lines passing through the reconstructed specimen. For each set of lines, the number of intersections were counted, and the MIL was defined as the total line length divided by the number of intersections. Using multiple regression, the components of the MIL matrix **M**, describing the MIL ellipsoid (Harrigan and Mann, 1984), were found. Assuming that the eigenvalues of the MIL matrix have the same standard deviation as its components, classification of the material was done by putting either a 90, 95 or a 99% confidence interval around the middle eigenvalue of the MIL matrix. The presence of the other two eigenvalues in the confidence interval decided whether orthotropy, transverse isotropy or isotropy was assumed. The eigenvectors of **M** give the directions of the axes of the ellipsoid, relative to the original coordinate system and thereby the assumed principal directions of the material were known.

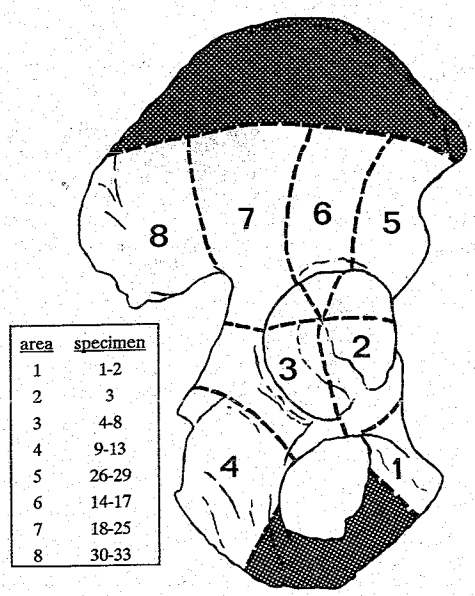

area	specimen
1	1-2
2	3
3	4-8
4	9-13
5	26-29
6	14-17
7	18-25
8	30-33

Fig. 1. Locations on the pelvic bone where the 33 specimens, used for combined mechanical testing and MIL measurements, were taken. The dotted areas denote the locations from which no specimens could be obtained due to lack of bone stock.

Calculation of the elastic constants

Tensor transformation was performed on the stress and strain tensors obtained for the mechanical test procedure to the principal directions obtained from the stereological measurement. As mentioned above, depending upon the statistical uniqueness of the eigenvalues of **M**, orthotropy, transverse isotropy or isotropy was assumed, which set the restrictions for the twelve nonzero components of the compliance matrix **S**. In case of orthotropy, the following equation should apply:

$$\begin{bmatrix} \varepsilon_1 \\ \varepsilon_2 \\ \varepsilon_3 \\ \varepsilon_4 \\ \varepsilon_5 \\ \varepsilon_6 \end{bmatrix} = \begin{bmatrix} S_{11} & S_{12} & S_{13} & 0 & 0 & 0 \\ S_{12} & S_{22} & S_{23} & 0 & 0 & 0 \\ S_{13} & S_{23} & S_{33} & 0 & 0 & 0 \\ 0 & 0 & 0 & S_{44} & 0 & 0 \\ 0 & 0 & 0 & 0 & S_{55} & 0 \\ 0 & 0 & 0 & 0 & 0 & S_{66} \end{bmatrix} \begin{bmatrix} \sigma_1 \\ \sigma_2 \\ \sigma_3 \\ \sigma_4 \\ \sigma_5 \\ \sigma_6 \end{bmatrix}.$$

For each specimen, three mechanical tests had been performed, so, for each ε_i and σ_i in the equation above, three values were known. In order to force-fit these data to a thermodynamically sound compliance matrix, separate singular value decompositions were then applied to the stress submatrices of the systems, given (in case of orthotropy) by the first three, the fourth, the fifth and the sixth rows of the above equation, respectively. The obtained pseudo-inverse stress matrices were multiplied by the respective strain submatrices, yielding the nine independent components of **S**. For isotropy and transverse isotropy, similar calculations were made, taking into account that for those cases, **S** contains only two and five independent

components, respectively. A more detailed description of the above procedure is given in Appendix I.

Depending upon the type of material behavior, Young's moduli, shear moduli and Poisson's ratios were calculated from the data of the mechanical tests and the MIL measurements according to Appendix I. Finally, for each confidence level considered to determine uniqueness of the eigenvalues of the MIL matrix, the calculated Young's and shear moduli were correlated to both the apparent density alone and a combination of apparent density and fabric components (Cowin, 1985), using nonlinear curvefitting.

RESULTS

Dual-energy quantitative computer tomography

Ca-equivalents for pelvic trabecular bone found with DEQCT varied between 0.04 and 0.22 $g cm^{-3}$. It appeared that the average Ca-equivalent value of the male bone was slightly, yet significantly ($p=0.05$) higher than the values of the female bones (0.13 $g cm^{-3}$ vs 0.09–0.11 $g cm^{-3}$). Figure 2 shows the average Ca-equivalents at the respective scan levels, averaged over the six pelvic bones. Statistical analysis (ANOVA) of this data revealed four areas where Ca-equivalents were significantly different ($p=0.05$) from each other; these being the ala of the iliac bone (1), the superior part of the acetabulum and the corpus of the iliac bone (2), the inferior part of the acetabulum, the ischial bone and the pubic–ischial junction (3) and, finally, the crista and the superior ramus of the pubic bone (4) (Fig. 2). Average values and standard deviations of the Ca-equivalents in these four areas are summarized in Table 1.

Mechanical testing

The average values of the apparent densities of the specimens were 0.345 $g cm^{-3}$ (S.D. 0.219 $g cm^{-3}$) in a range from 0.109 to 0.959 $g cm^{-3}$ for the female bone and 0.195 $g cm^{-3}$ (S.D. 0.054 $g cm^{-3}$) in a range from 0.114 to 0.314 $g cm^{-3}$ for the male bone. It may seem surprising that the female bone displayed a higher average bone density. This was mainly due to four of the female specimens with an apparent density of over 0.5 $g cm^{-3}$, which were taken from the superior acetabular area. When these four specimens were excluded as being subchondral bone rather than trabecular bone, the average apparent density for the female bone decreased to 0.248 $g cm^{-3}$ (S.D. 0.105 $g cm^{-3}$). Although still higher, this average density is not significantly different from the one found for the male bone. For both bones, the highest densities were found in the superior/anterior area of the

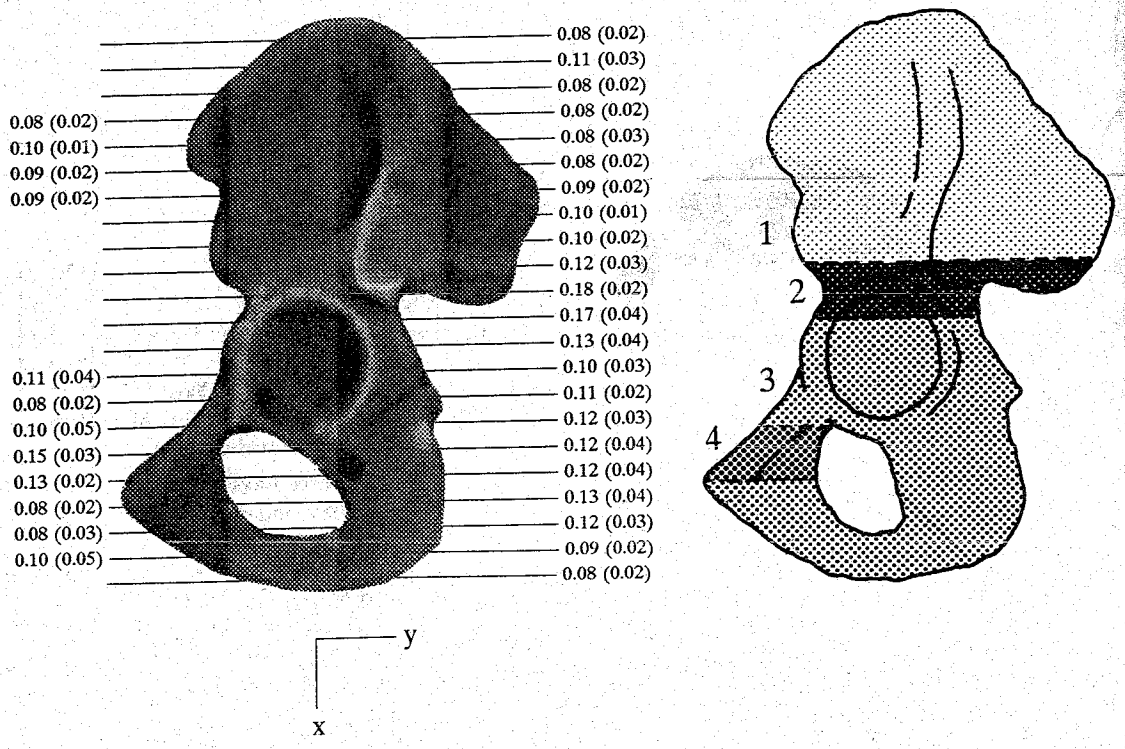

Fig. 2. Average Ca-equivalent densities and standard deviations (in $g cm^{-3}$) at every scan level and the identification of the areas between which the average Ca-equivalent densities were significantly different, based on six pelvic bones. (Those slices for which Ca-equivalents are indicated on the left side as well, had such a thin connection between the anterior and posterior trabecular bone mass (or even none) that separate anterior and posterior measurements were made.)

Table 1. The mean values and standard deviations of the Ca-equivalents in the four areas with statistically different bone densities of a pelvic bone

Area	Mean Ca-equivalent ($g\,cm^{-3}$)	S.D. Ca-equivalent ($g\,cm^{-3}$)
1	0.09	0.02
2	0.17	0.03
3	0.10	0.04
4	0.14	0.03

acetabular wall, while the lowest densities were found in the ischial bone.

Although, for the combination with the results of the MIL-measurements, only the stress and transverse strains at a longitudinal strain of 0.7% were needed, the elastic moduli in x-, y- and z-direction were calculated. In Fig. 3, these properties are represented as functions of the apparent density. The average elastic moduli in the x- and y-direction were not statistically different between both bones, the average elastic modulus in the z-direction for the female bone was slightly higher.

Stereological measurements

The low density of the specimens was reflected in the volume fractions (V_V), found by voxel counting. The average volume fraction was 10.8% (S.D. 3.6%). Correlating the apparent density to the volume fraction resulted in $\rho_{app} = 1.75\,V_V$ ($R^2 = 0.99$).

Visual representation of the three-dimensional specimen reconstructions showed a wide range of trabecular structures. There were specimens with an apparently direction-independent strut configuration, but also specimens with a well-defined texture of parallel plates (Fig. 4). A plate-like structure could be identified in about 70% of the cases. In none of these cases were the plates positioned parallel to the xy-plane, meaning that the plates were always found to be more or less perpendicular to the cortical shells.

Calculation of the elastic constants

Calculation of the elastic constants is dependent on the type of material behavior. Table 2 shows the distribution of the various types of material behavior, depending upon the confidence level used to determine statistical uniqueness of the eigenvalues of the MIL matrix found for the 33 specimens. It is obvious that a wider confidence interval implies that more specimens will be classified as isotropic. One of the specimens (no. 14) was actually classified differently at each of the three considered confidence levels. For this particular specimen, the actual procedure of calculating its elastic constants is worked out in Appendix II. Values of the elastic moduli, Poisson's ratios, the components of the fabric tensor and the ratio between the maximal and minimal Young's moduli (this being a measure for the degree of anisotropy) averaged over all 33 specimens together with the respective standard deviations are given in Table 3.

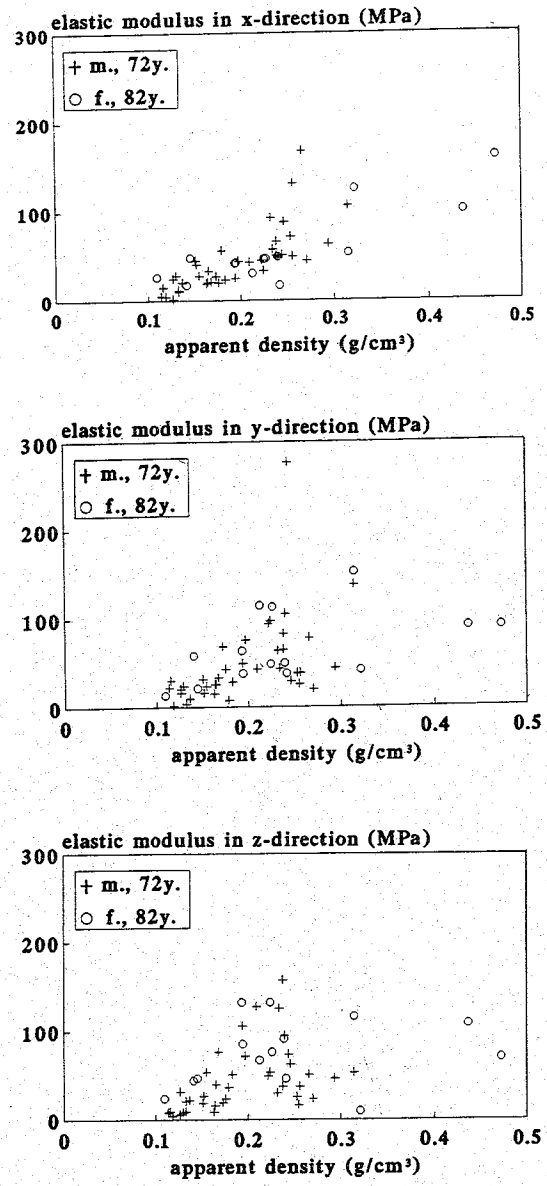

Fig. 3. Elastic moduli of the specimens from both the male and female donors in the x-, y- and z-direction as functions of the apparent density.

Returning to the four specimens shown in Fig. 4, their material behavior was classified, respectively, as oblately transversely isotropic ($E_1 = E_2 = 43.8$ MPa, $E_3 = 20.7$ MPa), isotropic ($E_1 = E_2 = E_3 = 23.6$ MPa), orthotropic ($E_1 = 167.0$ MPa, $E_2 = 64.6$ MPa, $E_3 = 58.9$ MPa) and prolately transversely isotropic ($E_1 = 96.0$ MPa, $E_2 = E_3 = 49.7$ MPa) at a confidence level of 95%.

Having information about the magnitudes and the directionality of the elastic properties of the tested specimens, it becomes possible to transpose this data back to the pelvic bone. Again for a confidence level of 95%, Fig. 5 shows the projections of the eigenvectors of the MIL matrix together with the calculated

Table 2. Occurrence of the various types of material behavior, depending upon the confidence level used to determine uniqueness of the eigenvalues of the MIL matrix for the 33 specimens

	Confidence level		
	90%	95%	99%
Orthotropy ($E_1 > E_2 > E_3$)	16	9	2
Prolate transversely isotropy ($E_1 > E_2 = E_3$)	5	3	3
Oblate transversely isotropy ($E_1 = E_2 > E_3$)	9	13	15
Isotropy ($E_1 = E_2 = E_3$)	3	8	13

Table 3. Average values and standard deviations (between brackets) of Young's moduli E_i (MPa), shear moduli G_{ij} (MPa), Poisson's ratio ν_{ij}, fabric components H_i and the ratio between E_1 and E_3 depending upon the confidence level used to determine uniqueness of the eigenvalues of the MIL matrix for the 33 specimens

	Confidence level		
	90%	95%	99%
E_1	61.6 (48.2)	59.8 (45.2)	59.8 (44.9)
E_2	42.4 (29.1)	50.1 (41.5)	57.3 (44.6)
E_3	31.0 (22.5)	38.3 (39.1)	43.2 (39.9)
G_{23}	18.4 (12.9)	20.8 (17.1)	22.6 (17.2)
G_{31}	23.4 (17.8)	23.5 (18.3)	22.6 (17.1)
G_{12}	25.7 (19.8)	25.2 (17.8)	26.0 (19.1)
ν_{21}	0.17 (0.12)	0.17 (0.10)	0.17 (0.10)
ν_{12}	0.24 (0.17)	0.20 (0.12)	0.18 (0.11)
ν_{31}	0.14 (0.07)	0.15 (0.08)	0.16 (0.07)
ν_{13}	0.27 (0.17)	0.26 (0.16)	0.24 (0.14)
ν_{32}	0.20 (0.14)	0.19 (0.13)	0.14 (0.09)
ν_{23}	0.28 (0.21)	0.27 (0.21)	0.21 (0.16)
H_1	0.390 (0.035)	0.377 (0.038)	0.365 (0.035)
H_2	0.334 (0.024)	0.341 (0.026)	0.346 (0.029)
H_3	0.276 (0.031)	0.282 (0.036)	0.346 (0.040)
E_1/E_3	2.0 (1.0)	1.7 (0.8)	1.4 (0.6)

Young's moduli for a number of specimens at their original locations in the pelvic bone.

Correlating Young's and shear moduli to apparent density and fabric components resulted in the following set of relations:

confidence level 90%:

$$E_i = 2017.3\ \rho_{app}^{2.46} \quad (R^2 = 0.58),$$

$$E_i = 15098.5\ \rho_{app}^{2.46}\ H_i^{1.80} \quad (R^2 = 0.69),$$

$$G_{ij} = 1012.1\ \rho_{app}^{2.44} \quad (R^2 = 0.62),$$

$$G_{ij} = 2049.1\ \rho_{app}^{2.44}\ (H_i + H_j)^{1.72} \quad (R^2 = 0.65),$$

confidence level 95%:

$$E_i = 1751.0\ \rho_{app}^{2.32} \quad (R^2 = 0.54),$$

$$E_i = 12261.9\ \rho_{app}^{2.33}\ H_i^{1.73} \quad (R^2 = 0.64),$$

$$G_{ij} = 938.8\ \rho_{app}^{2.38} \quad (R^2 = 0.61),$$

$$G_{ij} = 1534.0\ \rho_{app}^{2.39}\ (H_i + H_j)^{1.17} \quad (R^2 = 0.62),$$

confidence level 99%:

$$E_i = 1958.6\ \rho_{app}^{2.33} \quad (R^2 = 0.57),$$

$$E_i = 9162.7\ \rho_{app}^{2.34}\ H_i^{1.37} \quad (R^2 = 0.62),$$

$$G_{ij} = 919.4\ \rho_{app}^{2.35} \quad (R^2 = 0.61),$$

$$G_{ij} = 1084.2\ \rho_{app}^{2.35}\ (H_i + H_j)^{0.39} \quad (R^2 = 0.61).$$

Looking at the values of R^2, it can be seen that using only the apparent density as its predictor, the shear modulus shows a slightly better correlation than Young's modulus. However, adding the fabric components results in the opposite.

DISCUSSION

The purpose of this study was to find values for the elastic properties of pelvic trabecular bone. Assuming orthotropy as the highest degree of anisotropy, multiple tests on a single specimen would be required. This dictated the use of cubic specimens, even though the authors were well aware of the disadvantages and inaccuracies associated with this approach (Ashman *et al.*, 1989; Evans and King, 1961; Linde *et al.*, 1990a; Odgaard and Linde, 1991), causing an underestimation of Young's modulus relative to specimens with a larger length-to-area ratio. Bearing this in mind, nondestructive compressive tests were performed in three directions. However, it is not possible to obtain the shear moduli from these data. A solution for this could be to cut a smaller cube from the original under different angles and test this as well. Transformation of this second set of data into the directions of the first, makes it possible to find the values for the shear moduli (Snyder *et al.*, 1989). However, in our case an additional problem was the fact that the material's principal axes were not known beforehand. Cutting one smaller cube from the original would, therefore, not be sufficient and at least a third cube would be needed as well. But this would mean that the original specimens should be rather big. In fact, too big for trabecular bone specimens to be taken from the pelvic bone. Therefore, another approach was chosen. MIL measurements were performed on a digitized three-dimensionally reconstructed geometry of the specimens after mechanical testing. The axes of the MIL

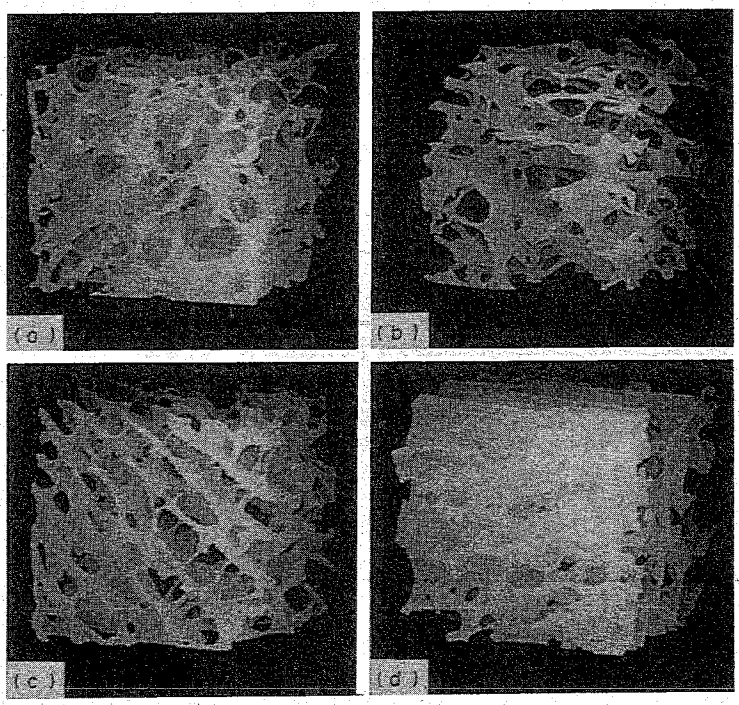

Fig. 4. Different appearances of pelvic trabecular structure in specimen no. 3 (a), specimen no. 4 (b), specimen no. 17 (c) and specimen no. 33 (d).

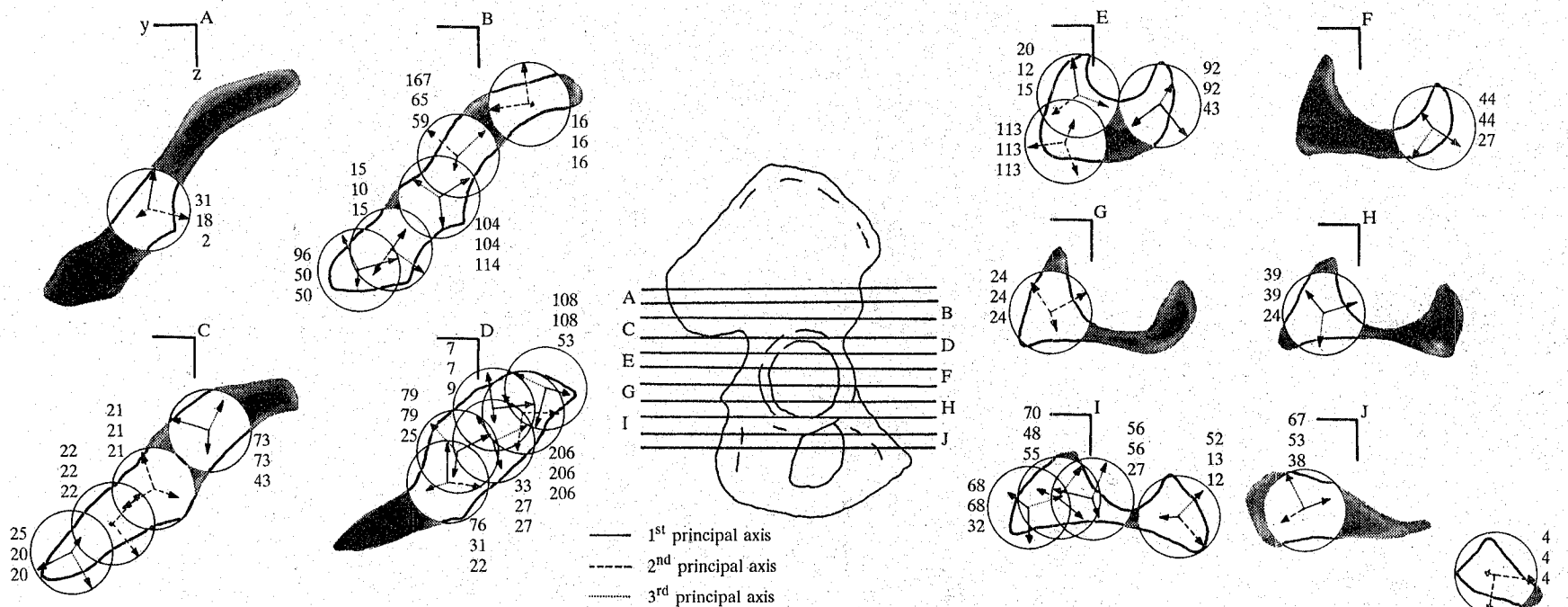

(Values Young's moduli in MPa)

Fig. 5. Projections of the principal material directions in the *yz*-plane (the out-of-plane components are directed in the positive *x*-direction) and magnitudes of Young's moduli in those directions for a number of specimens at their original location in the pelvic bone (confidence level 95%).

ellipsoid were assumed to be the same as the material's principal axes and the data from the mechanical tests were transformed in these directions. Using singular value decomposition on the relations for either orthotropic, transversely isotropic or isotropic behavior yielded three Young's moduli, three shear moduli and six Poisson's ratios.

Although none of the donors was known to have any history of bone or joint disease, their ages (72–87 yrs) alone contribute to the fact that low bone densities and consequently low elastic constants were found. However, as a part of the purpose of this study was to compare pelvic trabecular bone with trabecular bone from femoral and tibial origin, this aspect should have no effect. For the two pelvic bones used in this study for mechanical testing, trabecular bone with relatively low apparent densities was found. To support this finding, six other pelvic bones were used for bone densitometry measurements with a DEQCT method. The average Ca-equivalent densities at each scan level did not vary much between these six bones. The variation within a bone per scan level was such that four areas could be identified where Ca-equivalents were significantly different from adjacent areas (Fig. 2). The fact that the two high-density areas (upper part of the acetabulum to the sacroiliac joint area and the middle part of the pubic bone) coincide with the areas of major load transfer may, from a bone remodeling point of view, not come as a surprise. The apparent densities found for the two other bones, which were used for mechanical testing, suited well with these findings. Relating these apparent densities to the average Ca-equivalent densities locally measured to the six other bones, resulted in a positive correlation: $\rho_{Ca\text{-}eq} = 0.626\ \rho_{app}$ ($R^2 = 0.87$).

The values of the Ca-equivalent densities found in this study (0.04–0.22 g cm^{-3}) are quite similar to values of vertebral Ca-equivalent densities found by Lang *et al.* (1988) and Kalender *et al.* (1989). Other evidence for the resemblance between pelvic and vertebral trabecular bone are the values of the apparent densities of vertebral trabecular bone found by McBroom *et al.* (1985), lying in a range of 0.10–0.25 g cm^{-3}. These kind of values were also found in this study for the two pelvic bones used for mechanical testing. The average densities found for both male and female donors were not statistically different. These are indications that the densities found in this study are not exceptionally low, at least for donors in the age range used in this study (72–87 yr).

With apparent density (or volume fraction) as their primary predictor, the elastic constants that were found were low as well. For the majority of the specimens, the highest Young's modulus did not exceed 100 MPa. To some extent, this may be attributed to the methodology of mechanical testing. In the first place, cubic compression is known to underestimate Young's modulus, as already mentioned above. Furthermore, the fact that the specimens were tested unconstrained does also result in lower stiffnesses, but constrained testing would only have increased the stiffness by about 20% (Linde and Hvid, 1989). Multiple testing of the specimens, however, should not have had any major effect on the stiffness (Linde *et al.*, 1990b). But even taking these aspects into account, the elastic constants were significantly lower than values reported for specimens from the femoral head (Snyder *et al.*, 1989) or from the proximal tibia (Turner *et al.*, 1990), although it must be stated that in these studies the average age of the donors was lower (65 and 55 yr, respectively). However, our values for Young's moduli are again similar to values for vertebral trabecular bone (Lang *et al.*, 1988).

Looking back at the values assumed for Young's moduli for cancellous bone in various pelvic FE models, it appears that in most cases the values were too high. Pedersen *et al.* (1982) and Huiskes (1987) used values ranging from 1000 to 3000 MPa. Oonishi *et al.* (1983) used 1000 MPa in one study, while in another study 300 MPa was used (Oonishi *et al.*, 1986). Goel *et al.* (1978) also used a value of around 300 MPa. Only Vasu *et al.* (1982) and Rapperport *et al.* (1985) have used values which correspond to our findings, although their upper limits (1025 and 600 MPa, respectively) where high as well. It is worth noting that they were the only ones to base their Young's moduli on density distributions of actual pelvic bone (roentgenograms). The assumed value of 0.2 for Poisson's ratio of trabecular bone in nearly all studies mentioned above was shown by our study to be a good estimate. A Poisson's ratio of 0.2 was also found in other studies of trabecular bone from locations other than the pelvic bone.

Visual representation of the specimens that underwent the three-dimensional serial reconstruction, revealed a wide range of trabecular structures. In more than half of the specimens, a plate-like trabecular structure could be observed, whereby the plates were always more or less oriented perpendicular to the cortical shells. From a mechanical point of view, this is quite understandable, because as core material in a sandwich construction, pelvic trabecular bone will predominantly have to withstand shear-loading modes, against which a plate-like structure is the best resistance. Quantifying the degree of anisotropy depended on the statistical uniqueness of the eigenvalues of the MIL matrix. The smaller the confidence limit, the more specimens were classified as orthotropic. A rise in confidence level from 90 to 99% showed a decrease from 48 to 6% occurrence of orthotropic specimens. In case of transverse isotropy, the variant with two high-level moduli and one low-level modulus (oblate) was seen more often than the variant with one high-level modulus and two low-level moduli (prolate). This confirms the visual observation of the frequent occurrence of the plate-like structures. The two high-level moduli lie in the plane of the plate, while the low-level modulus is found in the connection rods. With this, pelvic trabecular bone

distinguishes itself from direct weight bearing (e.g. tibial) trabecular bone, where prolate transverse isotropy is found (high-level modulus in the weight bearing direction and the low-level moduli in the transverse directions). The ratio between the maximal and minimal Young's moduli (Table 3) reveals that pelvic trabecular bone is not highly anisotropic. This is confirmed by a minimal value of 0.315 for the second invariant of the fabric tensor, a measure of the degree of textural anisotropy, suggesting a maximal ratio of 1.9:1 between the major and minor orientation axes.

The statistical correlations between mechanical and textural properties are not as strong as reported in other studies (Hodgskinson and Currey, 1990; Snyder *et al.*, 1989; Turner, 1992 and Turner *et al.*, 1988, 1990). The exponent of the apparent density in the relations with both Young's modulus and the shear modulus varies between 2.3 and 2.5. With regard to the work of Gibson (1985), these values may be considered somewhat high. He points out that for low-density bone (open-celled structure) this relationship should be quadratic. In this study, however, despite the low densities, plate-like structures (closed-celled structure with a cubic relationship) were found relatively often, which might be the reason that the exponent lies between 2 and 3. For the fabric components this exponent shows a much broader range (0.4–1.8) and is strongly dependent on the confidence level used to determine uniqueness of the eigenvalues of the MIL matrix. This is plausible, as a higher confidence level implies relatively much isotropic behavior and for perfect isotropy the fabric components can not provide anymore relevant information. This can also be seen by the decreasing portion added to the R^2 when the fabric components are added in the correlations at increasing confidence levels. At a confidence level of 90%, adding H_i explains an extra 11% of the variance in Young's modulus, while at a level of 99% this percentage is reduced to 5%. For the shear modulus at 99%, even nothing seems to be gained by adding fabric components in the correlation. The fact that pelvic trabecular bone is not highly anisotropic and, therefore, does not show much variance in its fabric components, is the reason why, unlike Turner (1992), no higher exponents for the fabric components than 1.8 were found. The relatively high variances in the values of the elastic properties itself in combination with the wide range of observed bone structures seem to suggest that other textural properties than fabric or MIL are also needed in order to improve relations between elastic and textural properties.

Not having a direct weight bearing function, it can be concluded that pelvic trabecular bone consists of lower-density bone than trabecular bone in the femoral head or the proximal tibia. Consequently, the mechanical stiffness and strength (although the latter was not investigated here) will be lower. Its architecture displays a wide range of structures, although the predominant appearance is one of parallel plates. This accounts for the fact that transverse isotropic behavior with two high-level moduli and one low-level modulus is found relatively often.

REFERENCES

Ashman, R. B., Rho, J. Y. and Turner, C. H. (1989) Anatomical variation of orthotropic elastic moduli of the proximal human tibia. *J. Biomechanics* **22,** 895–900.

Cowin, S. C. (1985), The relationship between the elasticity tensor and the fabric tensor. *Mech. Mat.* **4,** 137–147.

Cowin, S. C. and van Buskirk, W. C. (1986) Thermodynamic restrictions on the elastic constants of bone. *J. Biomechanics* **19,** 85–87.

Dalstra, M. and Huiskes, R. (1990) The pelvic bone as a sandwich construction; a three dimensional finite element study. *Proc. ESB* **7,** B32.

Evans, F. G. and King, A. (1961) Regional differences in some physical properties of human spongy bone. In: *Biomechanical Studies of the Musculo-skeletal System* (Edited by Evans, F. G.), pp. 19–67. Charles C. Thomas Publisher, Springfield, IL.

Gibson, J. L. (1985) The mechanical behaviour of cancellous bone. *J. Biomechanics* **18,** 317–328.

Goel, V. K., Valliappan, S. and Svensson, N. L. (1978) Stresses in the normal pelvis. *Comput. Biol. Med.* **8,** 91–104.

Harrigan, T. P. and Mann, R. W. (1984) Characterization of microstructural anisotropy in orthotropic materials using a second rank tensor. *J. Mater. Sci.* **19,** 761–767.

Hodgskinson, R. and Currey, J. D. (1990) Effects of structural variation on Young's modulus of non-human cancellous bone. *Proc. Instn. Mech. Engrs.* **204,** 43–52.

Huiskes, R. (1987) Finite element analysis of acetabular reconstruction–non-cemented threaded cups. *Acta Orthop. Scand.* **58,** 620–625.

Kalender, W. A. and Suess, C. (1987) A calibration phantom for quantitative computed tomography. *Med. Phys.* **14,** 863–866.

Kalender, W. A., Felsenberg, D., Louis, O., Lopez, P., Klotz, E., Osteaux, M. and Fraga, J. (1989) Reference values for trabecular and cortical vertebral bone density in single and dual-energy quantitative computed tomography. *Eur. J. Radiol.* **9,** 75–80.

Lang, S. M., Moyle, D. D., Berg, E. W., Detorie, N., Gilpin, A. T., Pappas, N. J., Reynolds, J. C., Tkacik, M. and Waldron, R. L. (1988) Correlation of mechanical properties of vertebral trabecular bone with equivalent mineral density as measured by computed tomography. *J. Bone Jt Surg.* **70A,** 1531–1538.

Linde, F., Gøthgen, C. B., Hvid, I. and Pongsoipetch, B. (1988) Mechanical properties of trabecular bone by a non-destructive testing approach. *Engng Med.* **17,** 23–29.

Linde, F. and Hvid, I. (1989) The effect of constraint on the mechanical behaviour of trabecular bone specimens. *J. Biomechanics* **22,** 485–490.

Linde, F., Hvid, I. and Madsen, F. (1990a) The effect of specimen size and geometry on the mechanical behaviour of trabecular bone. *Proc. ESB* **7,** A25.

Linde, F., Pongsoipetch, B., Frick, L. H. and Hvid, I. (1990b) Three-axial strain controlled testing applied to bone specimens from the proximal tibial epiphysis. *J. Biomechanics* **23,** 1167–1172.

McBroom, R. J., Hayes, W. C., Edwards, W. T.., Goldberg, R. P. and White, A. A. (1985) Prediction of vertebral body compressive fracture using quantitative computed tomography. *J. Bone Jt Surg.* **67A,** 1206–1214.

Odgaard, A., Andersen, K., Melsen, F. and Gundersen, H. J. G. (1990) A direct method for fast three-dimensional serial reconstruction. *J. Microscopy* **159,** 335–342.

Odgaard, A. and Linde, F. (1991) The underestimation of Young's modulus in compressive testing of cancellous bone specimens. *J. Biomechanics* **24,** 691–698.

Oonishi, H., Isha, H. and Hasegawa, T. (1983) Mechanical analysis of the human pelvis and its application to the articular hip joint—by means of the three dimensional finite element method. *J. Biomechanics* **16,** 427–444.

Oonishi, H., Tatsumi, M. and Kawaguchi (1986) Biomechanical studies on fixations of an artificial hip joint acetabular socket by means of 2D-FEM. In: *Biological and Biomechanical Performance of Biomaterials* (Edited by Christel, P., Meunier, A. and Lee, A. J. C.), pp. 513–518. Elsevier, Amsterdam.

Pedersen, D. R., Crowninshield, R. D., Brand, R. A. and Johnston, R. C. (1982) An axisymmetric model of acetabular components in total hip arthroplasty. *J. Biomechanics* **15,** 305–315.

Rapperport, D. J., Carter, D. R. and Schurman, D. J. (1985) Contact finite element stress analysis of the hip joint. *J. orthop. Res.* **3,** 435–446.

Snyder, B. D., Cheal, E. J., Hipp, J. A. and Hayes, W. C. (1989) Anisotropic structure — property relations for trabecular bone. *ORS Trans.* **14,** 265.

Strang, G. (1986) *Introduction to Applied Mathematics*, Wellesley-Cambridge Press, Cambridge.

Turner, C. H., Rho, J. Y., Ashman, R. B. and Cowin, S. C. (1988) The dependence of the elastic constants of cancellous bone upon structural density and fabric. *ORS Trans.* **13,** 74.

Turner, C. H., Cowin, S. C., Rho, J.Y., Ashman, R. B. and Rice, J. C. (1990) The fabric dependence of the orthotropic elastic constants of cancellous bone. *J. Biomechanics* **23,** 549–561.

Turner, C. H. (1992) On Wolff's law of trabecular architecture. *J. Biomechanics* **25,** 1–9.

Vasu, R., Carter, D. R. and Harris, W. H. (1982) Stress distributions in the acetabular region — I. Before and after total joint replacement. *J. Biomechanics* **15,** 155–164.

APPENDIX I

One of the general descriptions of Hooke's law can be written as $\boldsymbol{\varepsilon}=\mathbf{S}\boldsymbol{\sigma}$, with S being the material's compliance matrix. From this, S can be solved if sufficient sets of $\boldsymbol{\varepsilon}$ and $\boldsymbol{\sigma}$ are available. Singular value decomposition is a standard means to calculate the pseudo-inverse of a nonsquare matrix (Strang, 1986), in this case $\boldsymbol{\sigma}$. Multiplying $\boldsymbol{\varepsilon}$ and $\boldsymbol{\sigma}^{-1}$ should yield S. However, in this particular case, only three sets of stresses and strains are available, which is not enough to solve the 21 unknown components of S. But, assuming the anisotropic material behavior to be either orthotropic, transverse isotropic or isotropic, already a lot about S is known, namely

$$\mathbf{S}_{\text{ortho}}=\begin{bmatrix} S_{11} & S_{12} & S_{13} & 0 & 0 & 0 \\ S_{12} & S_{22} & S_{23} & 0 & 0 & 0 \\ S_{13} & S_{23} & S_{33} & 0 & 0 & 0 \\ 0 & 0 & 0 & S_{44} & 0 & 0 \\ 0 & 0 & 0 & 0 & S_{55} & 0 \\ 0 & 0 & 0 & 0 & 0 & S_{66} \end{bmatrix},$$

$$\mathbf{S}_{\text{tr. iso}}=\begin{bmatrix} S_{11} & S_{12} & S_{12} & 0 & 0 & 0 \\ S_{12} & S_{22} & S_{23} & 0 & 0 & 0 \\ S_{12} & S_{23} & S_{22} & 0 & 0 & 0 \\ 0 & 0 & 0 & S_{44} & 0 & 0 \\ 0 & 0 & 0 & 0 & S_{55} & 0 \\ 0 & 0 & 0 & 0 & 0 & S_{66} \end{bmatrix}$$

or

$$\mathbf{S}_{\text{tr. iso}}=\begin{bmatrix} S_{11} & S_{12} & S_{13} & 0 & 0 & 0 \\ S_{12} & S_{11} & S_{13} & 0 & 0 & 0 \\ S_{13} & S_{13} & S_{33} & 0 & 0 & 0 \\ 0 & 0 & 0 & S_{44} & 0 & 0 \\ 0 & 0 & 0 & 0 & S_{44} & 0 \\ 0 & 0 & 0 & 0 & 0 & S_{66} \end{bmatrix}$$

and

$$\mathbf{S}_{\text{iso}}=\begin{bmatrix} S_{11} & S_{12} & S_{12} & 0 & 0 & 0 \\ S_{12} & S_{11} & S_{12} & 0 & 0 & 0 \\ S_{12} & S_{12} & S_{11} & 0 & 0 & 0 \\ 0 & 0 & 0 & S_{44} & 0 & 0 \\ 0 & 0 & 0 & 0 & S_{44} & 0 \\ 0 & 0 & 0 & 0 & 0 & S_{44} \end{bmatrix}.$$

For transverse isotropy, two separate cases are considered. In the first, the material is supposed to have one high-level Young's modulus and two equal low-level Young's moduli (prolate). In the second one, it is just the other way around, namely, two equal high-level moduli and one low-level modulus (oblate).

In the following, only the orthotropic case will be worked out further. For transverse isotropy and isotropy similar equations can easily be derived, which will be less elaborate, because in these cases, S has less independent components. As already stated above, singular value decomposition will not be used on the total system, but instead on our subsystems, these being

$$\begin{bmatrix} \varepsilon_1 \\ \varepsilon_2 \\ \varepsilon_3 \end{bmatrix}=\begin{bmatrix} S_{11} & S_{12} & S_{13} \\ S_{12} & S_{22} & S_{23} \\ S_{13} & S_{23} & S_{33} \end{bmatrix}\begin{bmatrix} \sigma_1 \\ \sigma_2 \\ \sigma_3 \end{bmatrix}$$

and

$$\varepsilon_i=S_{ii}\sigma_i \quad \text{for } i=4\text{–}6.$$

The first can be rewritten as

$$\begin{bmatrix} \varepsilon_1 \\ \varepsilon_2 \\ \varepsilon_3 \end{bmatrix}=\begin{bmatrix} \sigma_1 & \sigma_2 & \sigma_3 & 0 & 0 & 0 \\ 0 & \sigma_1 & 0 & \sigma_2 & \sigma_3 & 0 \\ 0 & 0 & \sigma_1 & 0 & \sigma_2 & \sigma_3 \end{bmatrix}\begin{bmatrix} S_{11} \\ S_{12} \\ S_{13} \\ S_{22} \\ S_{23} \\ S_{33} \end{bmatrix}.$$

In this equation, the 'extra' two sets of ε and σ are added rowwise, in the three other equations, the extra sets are added columnwise. Labeling the three sets of ε and σ with a, b and c, respectively, the following sets of equations remain to be solved:

$$\begin{bmatrix} \varepsilon_{1a} \\ \varepsilon_{2a} \\ \varepsilon_{3a} \\ \varepsilon_{1b} \\ \varepsilon_{2b} \\ \varepsilon_{3b} \\ \varepsilon_{1c} \\ \varepsilon_{2c} \\ \varepsilon_{3c} \end{bmatrix}=\begin{bmatrix} \sigma_{1a} & \sigma_{2a} & \sigma_{3a} & 0 & 0 & 0 \\ 0 & \sigma_{1a} & 0 & \sigma_{2a} & \sigma_{3a} & 0 \\ 0 & 0 & \sigma_{1a} & 0 & \sigma_{2a} & \sigma_{3a} \\ \sigma_{1b} & \sigma_{2b} & \sigma_{3b} & 0 & 0 & 0 \\ 0 & \sigma_{1b} & 0 & \sigma_{2b} & \sigma_{3b} & 0 \\ 0 & 0 & \sigma_{1b} & 0 & \sigma_{2b} & \sigma_{3b} \\ \sigma_{1c} & \sigma_{2c} & \sigma_{3c} & 0 & 0 & 0 \\ 0 & \sigma_{1c} & 0 & \sigma_{2c} & \sigma_{3c} & 0 \\ 0 & 0 & \sigma_{1c} & 0 & \sigma_{2c} & \sigma_{3c} \end{bmatrix}\begin{bmatrix} S_{11} \\ S_{12} \\ S_{13} \\ S_{22} \\ S_{23} \\ S_{33} \end{bmatrix}$$

and

$$[\varepsilon_{ia}\ \varepsilon_{ib}\ \varepsilon_{ic}]=S_{ii}[\sigma_{ia}\ \sigma_{ib}\ \sigma_{ic}] \quad \text{for } i=4\text{–}6.$$

Singular value decomposition applied to the matrices, containing the stress components in the above equations, will give their pseudo-inverses. Multiplying these by the respective strain matrices will yield the components of **S**, based on a multidimensional least-squares fit. In Appendix II, a numerical example of the above exercises will be given, using actual data of one of the specimens.

APPENDIX II

The calculation of the Young's and shear moduli and Poisson's ratios in the material's principal directions from the data of the mechanical tests and the MIL measurements for specimen no. 14 will be shown here as an example. This specimen happens to be classified as orthotropic at a 90% confidence level, transverse isotropic at 95% and isotropic at 99%. From the mechanical tests of this particular specimen follow the three pairs of stress and strain tensors (σ in MPa and ε in microstrain):

$$\boldsymbol{\sigma}_x = \begin{bmatrix} -0.172 \\ 0 \\ 0 \\ 0 \\ 0 \\ 0 \end{bmatrix}, \quad \boldsymbol{\varepsilon}_x = \begin{bmatrix} -7000 \\ 890 \\ 193 \\ 0 \\ 0 \\ 0 \end{bmatrix},$$

$$\boldsymbol{\sigma}_y = \begin{bmatrix} 0 \\ -0.344 \\ 0 \\ 0 \\ 0 \\ 0 \end{bmatrix}, \quad \boldsymbol{\varepsilon}_y = \begin{bmatrix} 1868 \\ -7000 \\ 1286 \\ 0 \\ 0 \\ 0 \end{bmatrix},$$

$$\boldsymbol{\sigma}_z = \begin{bmatrix} 0 \\ 0 \\ -0.741 \\ 0 \\ 0 \\ 0 \end{bmatrix}, \quad \boldsymbol{\varepsilon}_z = \begin{bmatrix} 1428 \\ 647 \\ -7000 \\ 0 \\ 0 \\ 0 \end{bmatrix}.$$

The MIL measurements and subsequent ellipsoid-fitting produced the following material anisotropy tensor **M**:

$$\mathbf{M} = \begin{bmatrix} 0.912 & 0.016 & -0.126 \\ 0.016 & 1.002 & -0.026 \\ -0.126 & -0.026 & 1.160 \end{bmatrix}.$$

The standard deviation in its components was 0.017. Eigenvalues and eigenvectors of **M** are

$$\lambda_1 = 0.859, \quad \mathbf{v}_1 = \begin{bmatrix} -0.923 \\ 0.033 \\ -0.384 \end{bmatrix},$$

$$\lambda_2 = 0.998, \quad \mathbf{v}_2 = \begin{bmatrix} 0.023 \\ -0.990 \\ -0.140 \end{bmatrix},$$

$$\lambda_3 = 1.217, \quad \mathbf{v}_3 = \begin{bmatrix} -0.385 \\ -0.138 \\ 0.913 \end{bmatrix}.$$

With a 90% confidence interval based on a standard deviation of 0.017 around λ_2 all three eigenvalues are distinct; so, then orthotropy is assumed. With a 95% confidence interval, λ_1 becomes trapped: so, here, transverse isotropy with two high-level moduli and one low-level modulus is assumed. Finally, with a 99% confidence interval also λ_3 is trapped and now isotropy is assumed.

The material's principal directions are defined by the eigenvectors of **M**. Transforming the above stress and strain tensors into these directions, results in

$$\boldsymbol{\sigma}_{x'} = \begin{bmatrix} -0.026 \\ -0.000 \\ -0.146 \\ 0.004 \\ -0.061 \\ 0.002 \end{bmatrix}, \quad \boldsymbol{\varepsilon}_{x'} = \begin{bmatrix} -859 \\ 873 \\ -5930 \\ 256 \\ -5114 \\ 316 \end{bmatrix},$$

$$\boldsymbol{\sigma}_{y'} = \begin{bmatrix} -0.007 \\ -0.337 \\ -0.000 \\ 0.011 \\ 0.002 \\ -0.047 \end{bmatrix}, \quad \boldsymbol{\varepsilon}_{y'} = \begin{bmatrix} 1216 \\ -6835 \\ 1772 \\ 518 \\ 488 \\ -2266 \end{bmatrix},$$

$$\boldsymbol{\sigma}_{z'} = \begin{bmatrix} -0.617 \\ -0.014 \\ -0.109 \\ -0.040 \\ 0.260 \\ -0.094 \end{bmatrix}, \quad \boldsymbol{\varepsilon}_{z'} = \begin{bmatrix} -5608 \\ 499 \\ 184 \\ -852 \\ 5915 \\ 1934 \end{bmatrix},$$

In case of orthotropy, these tensors are substituted in the appropriate equations as given in Appendix I. For the transverse isotropic and isotropic cases, similar sets of equations can be derived. Applying singular-value decomposition to obtain the pseudo-inverses of the stress submatrices, and multiplying these with the respective strain submatrices yield the values of S_{ij}. Having these values, the Young's and shear moduli and the Poisson's ratios are easily found using the relations worked out by Cowin and van Buskirk (1986). Their values are given in Table A1.

Despite the fact that the equations describing the material behavior were thermodynamically correct, it is due to the nature of the solution process using pseudo-inverse matrices (multidimensional least squares) that anomalies like $G_{23} > G_{12}$ may occur.

Table A1. Values of Young's moduli E_i (MPa), shear moduli G_{ij} (MPa) and Poisson's ratios ν_{ij}, depending upon the confidence level used to determine uniqueness of the eigenvalues of the MIL matrix for specimen no. 14

	Confidence level		
	90%	95%	99%
E_1	96.4	79.2	75.4
E_2	49.1	79.2	75.4
E_3	25.2	25.4	75.4
G_{23}	42.3	38.6	32.1
G_{31}	38.5	38.6	32.1
G_{12}	38.4	37.1	32.1
ν_{21}	0.06	0.07	0.18
ν_{12}	0.12	0.07	0.18
ν_{31}	0.17	0.16	0.18
ν_{13}	0.64	0.51	0.18
ν_{32}	0.12	0.16	0.18
ν_{23}	0.24	0.51	0.18